



































HAWC observations of the acceleration of very-high-energy cosmic rays in the Cygnus Cocoon

A. U. Abeysekara¹, A. Albert², R. Alfaro³, C. Alvarez⁴, J. R. Angeles Camacho³, J. C. Arteaga-Velázquez⁵, K. P. Arunbabu⁶, D. Avila Rojas³, H. A. Ayala Solares⁷, V. Baghmanyan⁸, E. Belmont-Moreno⁵, S. Y. BenZvi⁹, R. Blandford¹⁰ , C. Brisbois¹¹, K. S. Caballero-Mora⁴, T. Capistrán^{12,13} , A. Carramiñana¹², S. Casanova¹⁴ , U. Cotti⁵, S. Coutiño de León¹² , E. De la Fuente^{14,15} , R. Díaz Hernandez¹², B. L. Dingus², M. A. DuVernois¹⁶, M. Durocher¹² , J. C. Díaz-Vélez¹⁴ , R. W. Ellsworth¹¹, K. Engel¹¹ , C. Espinoza¹³ , K. L. Fan¹¹, K. Fang^{10,16} , H. Fleischhack¹⁷ , N. Fraija¹³ , A. Galván-Gómez¹³ , D. Garcia³, J. A. García-González³, F. Garfias¹³, G. Giacinti¹⁸ , M. M. González¹³ , J. A. Goodman¹¹ , J. P. Harding², S. Hernandez³, J. Hinton¹⁸, B. Hona¹ , D. Huang¹⁷, F. Hueyotl-Zahuantitla⁴ , P. Hüntemeyer¹⁷ , A. Iriarte¹³, A. Jardin-Blicq^{18,19,20} , V. Joshi²¹, D. Kieda¹ , A. Lara⁶ , W. H. Lee¹³, H. León Vargas³ , J. T. Linnemann²², A. L. Longinotti^{12,13}, G. Luis-Raya²³, J. Lundeen²², K. Malone¹² , O. Martinez²⁴, I. Martinez-Castellanos¹¹, J. Martínez-Castro²⁵, J. A. Matthews²⁶, P. Miranda-Romagnoli²⁷, J. A. Morales-Soto⁵, E. Moreno¹² , M. Mostafá⁷ , A. Nayerhoda⁸, L. Nellen²⁸, M. Newbold¹, M. U. Nisa²², R. Noriega-Papaqui²⁷, L. Olivera-Nieto¹⁸, N. Omodei¹⁰ , A. Peisker²², Y. Pérez Araujo¹³, E. G. Pérez-Pérez²³, Z. Ren¹² , C. D. Rho²⁹, D. Rosa-González¹², E. Ruiz-Velasco¹⁸, H. Salazar²⁴, F. Salesa Greus^{8,30} , A. Sandoval³, M. Schneider¹¹, H. Schoorlemmer¹⁸, F. Serna³, A. J. Smith¹¹, R. W. Springer¹, P. Surajbali¹⁸, K. Tollefson²², I. Torres¹² , R. Torres-Escobedo¹⁴, F. Ureña-Mena¹², T. Weisgarber³¹, F. Werner¹⁸, E. Willox¹¹ , A. Zepeda³², H. Zhou³³, C. De León⁵  and J. D. Álvarez⁵

Cosmic rays with energies up to a few PeV are known to be accelerated within the Milky Way^{1,2}. Traditionally, it has been presumed that supernova remnants were the main source of these very-high-energy cosmic rays^{3,4}, but theoretically it is difficult to accelerate protons to PeV energies^{5,6} and observationally there simply is no evidence of the remnants being sources of hadrons with energies above a few tens of TeV^{7,8}. One possible source of protons with those energies is the Galactic Centre region⁹. Here, we report observations of 1–100 TeV γ rays coming from the ‘Cygnus Cocoon’¹⁰, which is a superbubble that surrounds a region of massive star formation. These γ rays are likely produced by 10–1,000 TeV freshly accelerated cosmic rays that originate from the enclosed star-forming region Cyg OB2. Until now it was not known that such regions could accelerate particles to these energies. The measured flux likely originates from hadronic interactions. The spectral shape and the emission profile of the Cocoon changes from GeV to TeV energies, which reveals the transport of cosmic particles and historical activity in the superbubble.

The High-Altitude Water Cherenkov (HAWC) observatory is a wide field-of-view, very-high-energy γ -ray instrument that is sensitive in the energy range of 300 GeV to beyond 100 TeV. It is uniquely suited to the study of extended emission regions that contain bright background sources, as is the case for the Cygnus superbubble. A bright source, named 2HWC J2031+415 in the second HAWC catalogue¹¹ and shown in the significance map in Fig. 1, has been detected coincident with the superbubble. The location of this γ -ray emission overlaps with that of a known pulsar wind nebula (PWN) TeV J2032+4130 (ref. 12). Both TeV J2032+4130 and 2HWC J2031+415 are situated well within the extended region of γ -ray emission detected at GeV energies by the Fermi Large Area Telescope (Fermi-LAT)¹⁰. Another source, 2HWC J2020+403, possibly associated with the γ Cygni supernova remnant (SNR), lies 2.36° from the centre of 2HWC J2031+415.

By using 1,343 days of measurements with HAWC, we successfully removed the contribution of the overlapping sources to the TeV γ -ray emission in the region of interest (ROI) shown in Fig. 1. The 2HWC J2031+415 emission is well described by two sources: HAWC J2031+415 (at right ascension (RA) = 307.90° ± 0.04° and

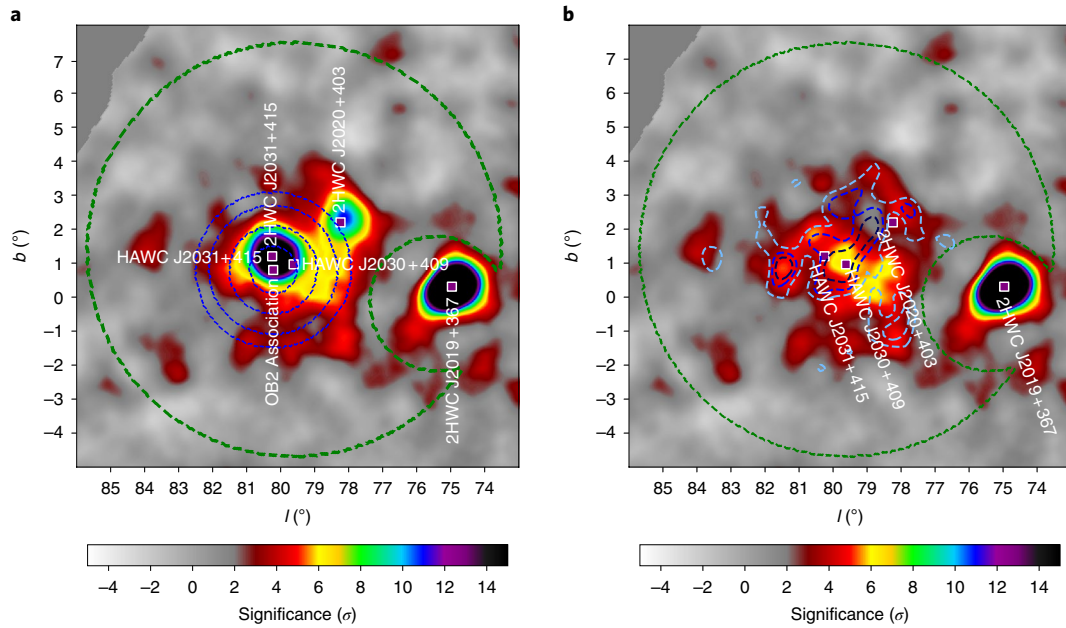


Fig. 1 | Significance map of the Cocoon region before and after subtraction of the known sources at the region. a, Significance map of the Cocoon region. The map is in Galactic coordinates, where b and l refer to latitude and longitude, respectively. It is produced as described in ref. ¹¹. The blue contours are four annuli centred at the OB2 association as listed in Supplementary Table 1. The green contour is the ROI used for the study, which masks the bright source 2HWC J2019+367. **b**, Significance map of the Cocoon region after subtracting HAWC J2031+415 (PWN) and 2HWC J2020+403 (γ Cygni). The light-blue, medium-blue and dark-blue dashed lines are contours for 0.16, 0.24 and 0.32 photons per $0.1^\circ \times 0.1^\circ$ spatial bin, respectively, from Fermi-LAT Cocoon¹⁰. Both maps are made assuming a 0.5° extended disk source and a spectral index of -2.6 with 1,343 days of HAWC data.

declination (dec.) = $41.51^\circ \pm 0.04^\circ$, which is a slightly extended source with a Gaussian width of 0.27° and is possibly associated with the PWN TeV J2032+4130 (refs. ^{12,13}), and HAWC J2030+409, which is a very-high-energy counterpart of the GeV Cygnus Cocoon¹⁰ (Methods). The region after subtraction of HAWC J2031+415 (PWN) and 2HWC J2020+403 (γ Cygni) is shown in Fig. 1b.

HAWC J2030+409 contributes $\sim 90\%$ to the total flux detected at the ROI and is detected with a test statistic (equation (1), likelihood ratio test), TS, of 195.2 at the position $RA = 307.65^\circ \pm 0.30^\circ$, $dec. = 40.93^\circ \pm 0.26^\circ$. The extension is well described by a Gaussian profile with a width of $2.13^\circ \pm 0.15^\circ$ (stat.) $\pm 0.06^\circ$ (syst.). The location and the Gaussian width of the source are consistent with the measurements by Fermi-LAT from above 1 GeV to a few hundred GeV.

The spectral energy distribution of the Cygnus Cocoon has been extended from 10 TeV in the previously published measurement by the ARGO observatory¹⁴ to 200 TeV in this analysis. The measurement above 0.75 TeV can be described by a power-law spectrum $dN/dE = N_0 (E/E_0)^\Gamma$, with $E_0 = 4.2$ TeV being the pivot energy. The flux normalization is $N_0 = 9.3^{+0.9}_{-0.8}$ (stat.) $^{+0.93}_{-1.23}$ (syst.) $\times 10^{-13} \text{ cm}^{-2} \text{ s}^{-1} \text{ TeV}^{-1}$ and the spectral index is $\Gamma = -2.64^{+0.05}_{-0.05}$ (stat.) $^{+0.09}_{-0.03}$ (syst.). The flux is compatible with an extrapolation from the Fermi-LAT measurement at 1–300 GeV (refs. ^{10,15}). Compared to $\Gamma = -2.1$ in the Fermi-LAT GeV data, a significant softening of the energy spectral density is evident at a few TeV in the ARGO data¹⁴ and persists beyond 100 TeV in the HAWC data (Fig. 2a).

GeV γ rays observed by Fermi-LAT can be produced either by high-energy protons interacting with gas or by high-energy electrons upscattering stellar radiation and dust emission¹⁰. Above a few TeV, the inverse-Compton process between relativistic electrons and stellar photons is suppressed by the Klein–Nishina effect. If produced by electrons, the γ -ray emission is therefore not expected

to be peaked toward the stellar clusters, but rather trace the diffuse dust emission across the entire Cocoon. This adds difficulty to the task of distinguishing the leptonic and hadronic origins of the γ -ray radiation. The measurements of the Cygnus Cocoon emission above 10 TeV break the degeneracy of the two origins. As shown in Extended Data Fig. 1, we find it unlikely that a single electron population produces γ rays from GeV to the highest energy by inverse-Compton emission without its synchrotron radiation violating the flux constraints posed by radio¹⁶ and X-ray¹⁷ observations. The leptonic origin of the γ -ray radiation by the Cygnus Cocoon is therefore disfavoured as uniquely responsible for the observed GeV and TeV flux.

The cosmic ray energy density above a proton energy of 10 TeV is calculated for four annuli up to 55 pc from Cyg OB2 (Fig. 2b). We find that the cosmic ray energy density in all spatial bins is larger than the local cosmic ray energy density of $10^{-3} \text{ eV cm}^{-3}$ based on Alpha Magnetic Spectrometer measurements¹⁸. Therefore, as for the GeV γ rays¹⁰, TeV γ rays come from the freshly accelerated cosmic rays inside the Cygnus Cocoon, rather than from the older Galactic population.

The radial profile of the cosmic ray density yields information on the mechanism that accelerates particles in the Cygnus Cocoon. Assuming that a cosmic ray accelerator has been active in the centre of the region at a radius of $r=0$, roughly at the location of Cyg OB2, a $1/r$ dependence of the cosmic ray density would imply that the acceleration process has continuously injected particles in the region for 1–7 Myr. A continuous acceleration process, which cannot be guaranteed by a single supernova explosion event, could be produced by the combined and long-lasting effect of multiple powerful star winds. Conversely, a constant radial profile would imply a recent (< 0.1 Myr) burst-like injection of cosmic rays, such as from a supernova explosion event. Although the measured cosmic ray profile seems to agree with a $1/r$ dependence, a constant profile, namely a burst-like injection, cannot be excluded. This is in contrast to the

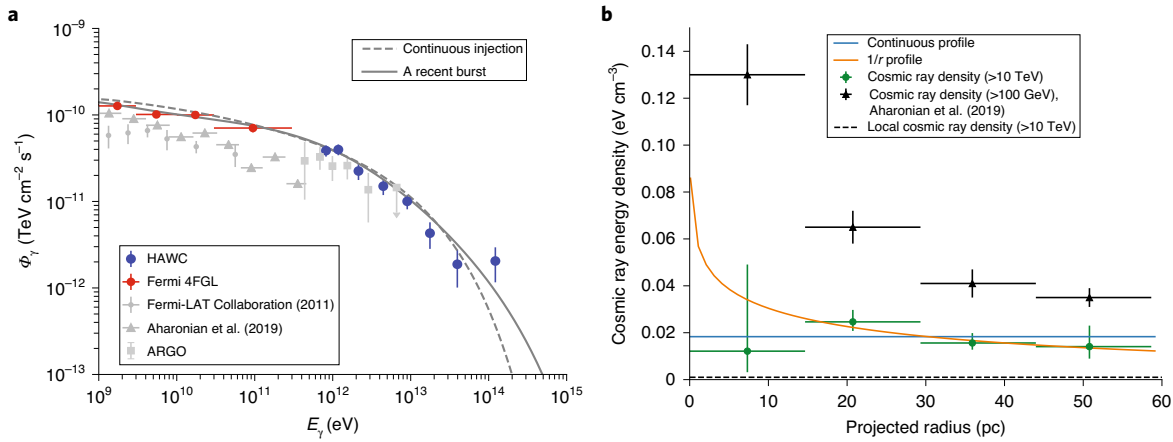


Fig. 2 | Spectral energy distribution of the γ -ray emission and cosmic ray density at the Cocoon region. **a**, Spectral energy distribution of the Cocoon measured by different γ -ray instruments. Here, Φ_γ is the γ -ray flux, which is given by $E_\gamma^2 \times dN/dE_\gamma$ and E_γ is the γ -ray energy. Blue circles are the spectral measurements for the Cocoon in this study. The errors on the flux points are the 1σ statistical errors. At low TeV energy, HAWC data agree with the measurements by the ARGO observatory shown in grey squares¹⁴. The red and grey circles are the Fermi-LAT flux points published in ref. ¹⁵ and ref. ¹⁰, respectively. The grey triangles are from the Fermi-LAT analysis in ref. ¹⁹. The grey solid and dashed lines are γ -ray spectra derived from the hadronic modelling of the region. (The leptonic modelling results are provided in Extended Data Fig. 1). **b**, Cosmic ray energy density profile calculated for four rings (0–15 pc, 15–29 pc, 29–44 pc and 44–55 pc) centred at the OB2 association. The green circles are the cosmic ray densities derived above 10 TeV using HAWC γ -ray data. The y errors are the statistical errors and the x error bars are the width of the x bins. The orange and blue lines are the $1/r$ profile (signature of the continuous particle injection) and constant profile (signature of the burst injection), respectively, calculated by assuming a spherical symmetry for the γ -ray emission region and by averaging the density profile over the line of sight within the emission region. The black dashed line is the local cosmic ray density above 10 TeV based on Alpha Magnetic Spectrometer measurements¹⁸. The black triangles are the cosmic ray densities above 100 GeV from ref. ¹⁹.

cosmic ray density profile above 100 GeV from ref. ¹⁹, which clearly favours the $1/r$ profile. Alternatively, the $1/r$ profile is less striking for TeV cosmic rays because of their escape time.

The angular size of the Cygnus Cocoon is about 2.1° , which translates into a radius of $r = 55$ pc at 1.4 kpc. The size of the Cocoon is similar in both the TeV and GeV energy range. Assuming a loss-free regime, the particles from tens of GeV to hundreds of TeV diffuse in the region over a time t_{diff} given by $t_{\text{diff}} = r^2/(2D)$ (ref. ²⁰), where D is the particle diffusion coefficient. If $D(E) = \beta D_0(E)$, where $D_0(E)$ is the average diffusion coefficient in the Galaxy at a given energy E and β is the suppression coefficient, then at 10 GeV

$$t_{\text{diff}}(10 \text{ GeV}) = 15,000 \times \left(\frac{1}{\beta}\right) \times \left(\frac{R_{\text{diff}}}{55 \text{ pc}}\right)^2 \times \left(\frac{D_0(10 \text{ GeV})}{3 \times 10^{28} \text{ cm}^2 \text{ s}^{-1}}\right)^{-1} \text{ yr}.$$

The diffusion time (t_{diff}) of 10 GeV particles detected with Fermi-LAT needs to be shorter than the age of the Cyg OB2 association t_{age} , that is, $t_{\text{diff}}(10 \text{ GeV}) < t_{\text{age}} \approx 1\text{--}7$ Myr (ref. ²¹), which yields $\beta > 0.002$. By contrast, the diffusion time of 100 TeV particles must be longer than the light-travel time to the edges of the Cocoon, $t_{\text{diff}}(100 \text{ TeV}) \gg R_{\text{diff}}/c$, where R_{diff} is the diffusion radius and c is the speed of light. With $D_0(100 \text{ TeV}) = 3 \times 10^{30} \text{ cm}^2 \text{ s}^{-1}$, we obtain $\beta \ll 1$. The combination of observations by the GeV and TeV instruments provides unique insights to particle transport in the Cocoon superbubble. The ‘suppression of the diffusion coefficient’ (β) is found to be $0.002 < \beta \ll 1$. This confirms that closer to particle injectors, high turbulence is driven by the accelerated particles, and cosmic rays are likely to diffuse more slowly than in other regions of the Galaxy.

As discussed in ref. ¹⁰, although the PWN powered by PSR J2021+4026 and PSR J2032+4127 cannot explain this extended Cocoon emission, we cannot rule out that the emission could be from a yet-undiscovered PWN. The nearby γ Cygni SNR might not have been able to diffuse over the Cocoon region because of its young age¹⁰. The γ -ray emission measured from the Cocoon

region over five orders of magnitude in energy is likely produced by protons in the GeV to PeV range that collide with the ambient dense gas. The spectral shape in the TeV energy range is well described by a power law without an indication of a cut-off up to energies above 100 TeV. Therefore, it might be the case that the powerful shocks produced by multiple strong star winds in the Cygnus Cocoon can accelerate particles, not only to energies up to tens of TeV as previously indicated by the Fermi-LAT detection, but even beyond PeV energies. However, the presence of a cut-off or a break in the GeV to TeV γ -ray spectrum at a few TeV, as evidenced in the measurements of both ARGO and HAWC detectors, argues against the efficiency of the acceleration process beyond several hundred TeV.

The break in the γ -ray spectrum around a few TeV could be due to either leakage of cosmic rays from the Cocoon or a cut-off in the cosmic ray spectrum injected from the source. In the first scenario, the γ -ray emission is dominated by recent starburst activities less than 0.1 Myr ago. The diffusion length in the Cocoon is 100–1,000 times less than that in the interstellar medium owing to strong magnetic turbulence¹⁰ that is plausibly driven by starburst activities. The lower-energy cosmic rays are confined by the magnetic field of the Cocoon, whereas higher-energy cosmic rays escape from the region before producing γ rays, which results in a spectral break from GeV to TeV regime. An injection index of $\alpha \approx -2.1$ for the cosmic ray spectrum is needed to explain the Fermi-LAT observation. Such a spectrum can be achieved by different particle acceleration mechanisms, for example through shock acceleration. An example of the leakage model is illustrated as the thick solid grey line in Fig. 2a. Assuming a recent activity that happened 0.1 Myr ago and a gas density of 30 nucleons per cm^3 as suggested by H I and H II observations²², the proton injection luminosity is found to be $L_p \approx 4 \times 10^{37} \text{ erg s}^{-1}$ above 1 GeV (Methods). The data above 100 TeV suggest that the stellar winds inject protons to above PeV with a hard spectrum.

In the second scenario, the γ -ray emission is produced by continuous starburst activities over the OB2 star lifetime, 1–7 Myr. In this scenario, a hard cosmic ray spectrum of $\alpha \approx -2.0$, depending on the

index of the turbulence, is required to meet the γ -ray spectrum of $\gamma \approx -2.1$ at GeV energies. As illustrated by the dashed grey curve in Fig. 2a, a cut-off in the injected proton energy around 300 TeV can explain the change of spectral index from GeV to TeV regime. This scenario requires a proton injection luminosity of $L_p \approx 7 \times 10^{36} \text{ erg s}^{-1}$ above 1 GeV.

The total mass of the OB2 association is $2\text{--}10 \times 10^4 M_\odot$ (refs. 23,24), and the wind mechanical luminosity is estimated to be $\sim 1\text{--}2 \times 10^{39} \text{ erg s}^{-1}$ (ref. 23). The stellar association therefore requires 4% and 0.7% acceleration efficiency for the burst model and the steady model, respectively. OB2 produces sufficient power to account for the acceleration of cosmic rays that now make up the Cocoon.

The HAWC observation reveals the high-energy spectrum of Cygnus Cocoon, a representative of one of the most plausible Galactic cosmic ray source classes, at the highest γ -ray energies. The TeV measurements provide direct evidence that the Cygnus Cocoon accelerates cosmic ray protons above 100 TeV. When we compare with the GeV Cocoon measurements¹⁰, we do not observe a hard γ -ray spectrum above 1 TeV. Although the γ -ray emission of superbubbles turns out to be more complicated than previously understood, we show that the Cocoon may still be a PeVatron if the break in the energy spectrum is caused by the escape of higher-energy cosmic rays. Our result suggests that Cygnus Cocoon could also emit high-energy neutrinos that are created by the decay of ions produced by hadronic interactions of the cosmic ray protons with the gas density in the ambient region. Although these neutrinos have not been detected yet, they may be identified through extended source analysis by IceCube and future neutrino experiments^{25,26}. The feasibility of these neutrino detections could be evaluated by using a hadronic γ -ray emission template based on the TeV Cocoon model. Future very-high-energy γ -ray observations such as SWGO²⁷ and LHAASO²⁸ will provide more statistics that can be used to resolve the contribution of other stellar clusters to Galactic cosmic rays around the knee of the energy spectrum.

Methods

The HAWC Observatory. The HAWC γ -ray instrument consists of an array of 300 water Cherenkov detectors at an altitude of 4,100 m in Sierra Negra, Mexico. It is sensitive to γ rays in the energy range of a few hundred GeV to beyond 100 TeV (ref. 29). Each water Cherenkov detector has four photomultiplier tubes at the bottom that detect the Cherenkov light produced by air shower particles travelling through the detector. Air shower events recorded by the detector are reconstructed to extract shower properties. The hadronic cosmic rays that pass gamma/hadron separation cuts during the reconstruction are the main background in the analysis of γ -ray sources³⁰. The background is computed as in ref. 29.

HAWC data are divided into nine size bins according to the fraction of photomultiplier tubes triggered in a shower event. Size bin 9 has the highest-energy γ rays and the best angular resolution of 0.17° (68% containment radius) or better³⁰. Each size bin is further subdivided into 12 quarter-decade energy bins for a total of 108 bins (ref. 29) by using the 'ground parameter' energy estimation algorithm, which uses the charge density at 40 m from the shower axis²⁹. The results presented here are based on 1,343 days of data collected between June 2015 and February 2019 for events with energies that were reconstructed above 1 TeV by the 'ground parameter' method²⁹.

Model fitting at the Cocoon region. A model describing the sources in the Cocoon region is fitted by using the maximum-likelihood code 3ML (ref. 31). This method estimates the best-fit value for the parameters being fitted for the spatial and spectral description of the model to maximize the likelihood of the model. Given the model, the expected γ -ray events and background events are calculated by forward folding with the detector response. A test statistic (TS) of each source is then defined as the log of the ratio of the maximum likelihood of the best-fit model including the source $L_{(\text{source})}$ in question to the likelihood of the best-fit model without that source $L_{(\text{no source})}$:

$$\text{TS} = 2 \ln \frac{L_{(\text{source})}}{L_{(\text{no source})}}. \quad (1)$$

The region of interest used for the fit is a disk of radius 6° centred at RA = 307.17° and dec. = 41.17° with a 2° mask around the bright Cygnus region source 2HWC J2019+367 (ref. 11) (eHWC J2019+368 (ref. 33)). The best-fit description of the γ -ray emission in the ROI includes three sources. Two sources,

HAWC J2031+415 and HAWC J2030+409, together contribute to the emission detected at the 2HWC J2031+415 region³³. HAWC J2031+415 is possibly associated with the PWN TeV J2032+4130, which is the first extended γ -ray source detected in the range of very high energies¹². After the discovery by HEGRA, the detection has been confirmed by various observatories^{34–37}. The γ -ray emission is likely a PWN powered by PSR J2032+4127 (ref. 37). HAWC J2030+409 is a TeV counterpart of the Fermi-LAT Cocoon¹⁰. The ROI also includes a nearby third source 2HWC J2020+403 (γ Cygni), which is possibly associated with VER J2019+407 (ref. 38), enclosed within the radio shell of the γ Cygni SNR. The three sources account for all of the TeV emission observed in the ROI region. The spectral fit results for these three sources along with the TS values are provided in Supplementary Table 2. The profile of the emission centred at the HAWC J2030+409 is given in Supplementary Fig. 1b, where the blue line represents the model after subtracting PWN and γ Cygni.

Different spectral models were explored for HAWC J2030+409 (HAWC Cocoon), namely a power-law spectrum

$$\frac{dN}{dE} = N_0 \left(\frac{E}{E_0} \right)^{\Gamma}, \quad (2)$$

and a power law with an exponential cut-off

$$\frac{dN}{dE} = N_0 \left(\frac{E}{E_0} \right)^{\Gamma} \times \exp(-E/E_c). \quad (3)$$

The pivot energy E_0 is fixed at 4.2 TeV for both equations (2) and (3). The free parameters are N_0 and Γ . In addition, the Gaussian width is fitted. The two equations (2) and (3) constitute nested models. With Wilks' theorem³⁹ to convert ΔTS to a significance, there is no significant improvement in the TS value for a spectral fit using equation (3) (TS = 196.9) compared to using equation (2) (TS = 195.2). Hence, for the HAWC J2030+409 spectrum, there is no significant preference for a cut-off in the spectrum in comparison to a simple power-law spectrum. The TeV Cocoon spectrum is therefore described by a power-law spectrum. The likelihood profile of the cut-off energy assuming a power-law spectrum with an exponential cut-off for the Cocoon is shown in Supplementary Fig. 1a. At a 95% confidence level, the lower limit to a cut-off is obtained at 15 TeV.

The HAWC J2031+415 (PWN) is described by a power-law spectrum with an exponential cut-off and Gaussian morphology. A power-law spectrum with an exponential cut-off is chosen as it is preferred in our model in comparison to a power-law spectrum by a ΔTS of 16.9 ($\sim 4\sigma$). The TS values for the PWN for a simple power-law spectrum and for a power law with an exponential cut-off are 281.6 and 298.5, respectively. The free parameters are flux normalization N_0 , index Γ and cut-off energy E_c of equation (3), plus the Gaussian width. The 2HWC J2020+403 (γ Cygni) is described by a power-law spectrum with a disk radius fixed at 0.63° based on the studies of ref. 40. The free parameters are N_0 and Γ of equation (2).

Residual significance distribution. The significance distributions in the ROI before and after subtracting various sources are shown in Supplementary Fig. 2. If the residual map obtained after subtracting the model contains only background fluctuations, then the significance histogram should follow a normal distribution. The dotted lines in the plots are the expected and the obtained distribution.

The significance map with the ROI circled in green is shown in Fig. 1. The significance distribution obtained for the ROI (Supplementary Fig. 2a) is skewed towards positive values owing to the presence of different γ -ray sources. Because of these sources, we see excess counts above background fluctuations. After subtraction of the PWN and the γ Cygni SNR, the skew is considerably reduced (Supplementary Fig. 2b). The excess counts from the Cocoon source contribute to this skew. Finally, when the Cocoon source in addition to the PWN and γ Cygni are subtracted, there are no longer significant excess counts over background fluctuations (Supplementary Fig. 2c).

Energy range. A method similar to the energy range method in ref. 41 is applied to determine the energy range of γ -ray emission from the TeV Cocoon. The best-fit model (the power-law spectrum of equation (2)) is multiplied by a step function at some value to simulate a sharp cut-off in energy. The free parameters are the strict upper or lower cut-off for the energy in addition to the flux normalization and index of the Cocoon. The energy value at which the log likelihood decreases by 1σ from the maximum log likelihood value in the nominal case (Supplementary Fig. 3) is then quoted as the lower limit to the maximum detected γ -ray energy (when the free parameter is a strict upper cut-off) or as the upper limit to the minimum detected γ -ray energy (when the free parameter is a strict lower cut-off).

Based on the energy range studies, the TeV Cocoon spectrum extends from 0.75 TeV to 225 TeV. The TS values for the Cocoon in each median reconstructed energy are provided in Supplementary Table 3. The TS above 100 TeV is about 6.

Cosmic ray density profile. The annular rings used in the density profile study are similar to the annular bins used in ref. 19. The four rings 0–0.6°, 0.6–1.2°, 1.2–1.8° and 1.8–2.2° (corresponding to 0–15 pc, 15–29 pc, 29–44 pc and 44–55 pc,

respectively), centred at the position of the OB2 association (308.3°, 41.3°), are selected as illustrated in Fig. 1a. With the 3ML software³¹, the four rings are fit simultaneously with the contributions from PWN and γ Cygni. In total, this six-source (four rings, PWN and γ Cygni) model has 13 free parameters (flux normalization and index of the four rings; flux normalization, index and cut-off energy of the PWN; and flux normalization and index of γ Cygni). With the integral flux (I_{ring}) for each ring from ~ 1 TeV to ~ 200 TeV, the total luminosity of each ring is calculated as

$$L_{\gamma} = 4\pi I_{\text{ring}} \times d^2, \quad (4)$$

where d is the distance to the OB2 association (1.4 kpc (ref. ⁴³)). Gas mass (M) in the region is also used as quoted in ref. ¹⁹, and the cosmic ray density w_{CR} can be calculated by using the formula in equation (5) (ref. ⁹):

$$w_{\text{CR}}(>10 \text{ TeV}) = 1.8 \times 10^{-2} \left(\frac{\eta}{1.5} \right)^{-1} \frac{L_{\gamma}(\geq 1 \text{ TeV})}{10^{34} \text{ erg s}^{-1}} \left(\frac{M}{10^6 M_{\odot}} \right)^{-1} \text{ eV cm}^{-3} \quad (5)$$

η accounts for the presence of the heavier-than-hydrogen nuclei and is taken to be 1.5 (refs. ^{43,44}). Then, with equation (5), the density values w_{CR} above 10 TeV are given in Supplementary Table 1. In Fig. 2b, the green circles represent cosmic ray energy density against the distance from the centre of the OB2 association, and the average cosmic ray density profiles over the line of sight are shown as orange and blue lines. The reduced chi squared χ^2 is 1.12 for a constant profile and 0.46 for $1/r$ profile. Owing to the large statistical errors, the study cannot provide conclusive evidence of $1/r$ signature for continuous injection versus constant profile for burst-like injection. According to ref. ¹⁹, the systematic uncertainties associated with the gas mass in the Cocoon region could be as high as 50%. Adding the systematic error of $\pm 50\%$ in the gas mass does not alter our conclusion that our study cannot claim a preference for continuous injection versus burst-like injection.

Hadronic modelling. Protons interact with the ambient gas cloud and produce π^0 which immediately decays into γ rays. The expected γ -ray flux from the parent proton flux in the Cocoon are shown in Fig. 2a. We assume a 59.2 mb cross-section for the p-p interaction between a PeV proton and a rest-mass proton⁴⁵. The gas density of the Cocoon region is approximately 30 nucleons per cm^3 (ref. ²²).

Transient source. Here, we consider a starburst event at t_0 that injects particles with rate $Q(E, t) = S(E) \delta(t - t_0)$, where $S(E) \equiv S_0 E^{-\alpha} \exp(-E/E_{\text{cut}})$ depends only on energy and α is the spectral index. The solution of the cosmic ray transport equation applied to the Cocoon region is⁴⁶

$$n(E, r, t - t_0) = \frac{b(E_0)}{b(E)} S(E_0) \frac{\exp[-r^2/(4\lambda_0^2)]}{(4\pi\lambda_0^2)^{3/2}}, \quad (6)$$

where E_0 is the initial proton energy at t_0 and $b(E) = dE/dt$ is the energy loss rate. λ_0 is the distance travelled by the particle when its energy decreases from E_0 to E (or from time t_0 to time t) and is a function of particle diffusion coefficient $D(E)$:

$$\lambda_0 = \left[\int_E^{E_0} \frac{D(\epsilon)}{b(\epsilon)} d\epsilon \right]^{1/2}. \quad (7)$$

Assuming that the proton density inside the Cocoon is from a source at the centre, the total number of cosmic rays from a burst at t_0 is

$$\frac{dN}{dE}(t - t_0) = \frac{b(E_0)}{b(E)} S(E_0) F_{\text{cc}}(E, t_0) \quad (8)$$

$$= \frac{E_0}{E} S_0 E^{-\alpha} \exp(-E/E_{\text{cut}}) F_{\text{cc}}(E, t_0) \quad (9)$$

where F_{cc} depends on the radius of the Cocoon ($R_{\text{cc}} = 50$ pc) and the time of the burst:

$$F_{\text{cc}} = \text{erf}\left(\frac{R_{\text{cc}}}{2\lambda_0}\right) - \frac{1}{\pi^{1/2}} \frac{R_{\text{cc}}}{\lambda_0} \exp[-R_{\text{cc}}^2/(4\lambda_0^2)]. \quad (10)$$

For the turbulent magnetic field in the Cocoon, $D(E) = 10^{25}(E/1 \text{ GeV})^{0.55} \text{ cm}^2 \text{ s}^{-1}$ is adopted. Fitting the function with the 4FGL Cocoon flux points¹⁵ and HAWC data, the initial injection rate S_0 for $t_0 = 0.1$ Myr obtained is $\sim 9 \times 10^{37} \text{ erg s}^{-1}$. We find the best-fitted injected proton spectrum with spectral index $\alpha = -2.13$ with E_{cut} fixed at ~ 100 PeV. The result is insensitive to the value of E_{cut} as long as it is above ~ 1 PeV.

The proton luminosity (L_p) is then calculated as

$$L_p = \int_{E_{\text{min}}}^{E_{\text{max}}} Q_0 E^{-\alpha} \exp(-E/E_{\text{cut}}) dE. \quad (11)$$

For $E_{\text{min}} = 1$ GeV and $E_{\text{max}} = 1$ PeV, $L_p \approx 4 \times 10^{37} \text{ erg s}^{-1}$.

Steady source. If the source injects particles continuously in time with a temporal profile $Q(t)$, the cosmic ray flux sums the contribution from different injection episodes.

$$\frac{dN}{dE}(t) = \int_0^{\tau_{\text{cc}}} dt_0 \frac{dN}{dE}(t - t_0) Q(t_0) \quad (12)$$

where τ_{cc} is the source age. With $\tau_{\text{cc}} = 3$ Myr, the initial injection rate $Q(t_0)$ obtained is $\sim 1 \times 10^{36} \text{ erg s}^{-1}$. The best spectral fit has a spectral index of $\alpha = -2.0$ and a cut-off E_{cut} fixed at ~ 300 TeV. For the steady source, $D(E) = 10^{25}(E/1 \text{ GeV})^{0.33} \text{ cm}^2 \text{ s}^{-1}$ is adopted. With $E_{\text{min}} = 1$ GeV and $E_{\text{max}} = 300$ TeV, $L_p \approx 7 \times 10^{36} \text{ erg s}^{-1}$.

Assuming a 0.7% to 4% acceleration efficiency from the proton injection luminosity obtained here for the two models, to generate $0.3\text{--}1 \times 10^{41} \text{ erg s}^{-1}$ power to explain the energy density of Galactic cosmic rays⁴⁷, $\sim 10^4$ Cyg OB2-like stellar associations would be required. Currently, fewer than 100 OB associations (Cyg OB2 being the most massive) have been identified in the 3 kpc survey of our Galaxy^{48,49}.

Both of these models (transient source and steady source) adequately describe the observed GeV to TeV data. Given the current statistical errors, we cannot provide conclusive evidence that one model should be preferred over the other.

The γ -ray flux produced by protons injected at t_0 is

$$\Phi_{\gamma}(E_{\gamma}, t) = \frac{cn_{\text{H}}}{4\pi D_{\text{cc}}^2} \int_{E_{\gamma}}^{\infty} dE_p \sigma_{\text{pp}}(E_p) \left[F_{\gamma}\left(\frac{E_p}{E_{\gamma}}, E_p\right) \frac{1}{E_p} \right] \frac{dN_p}{dE_p}(t - t_0), \quad (13)$$

where $F_{\gamma}(E_p/E_{\gamma}, E_p)$ is the spectrum produced by one proton with energy E_p via π^0 decay and n_{H} is the proton density. An analytical form of F_{γ} is presented in equation (58) of ref. ⁴⁵. The transition of propagation regimes⁵⁰ may also lead to features in a γ -ray spectrum, but cannot explain the spectral change around 1 TeV observed from the Cygnus Cocoon, as proton propagation at these energies is still in the diffusive regime.

Leptonic modelling. The electron spectrum is computed by solving the following transport equation:

$$\frac{\partial n(E, r)}{\partial t} - \nabla[D(E) \nabla n(E, r)] - \frac{\partial}{\partial E}[b(E) n(E, r)] = Q(E, t) \delta(r) \quad (14)$$

where $D(E) = D_0 E^{\delta}$ is the diffusion coefficient with $\delta \approx 0.33$ for the Kolmogorov turbulence, $Q(E, t) = Q_0 E^{-\alpha}$ is the particle injection rate and $b(E) = dE/dt$ is the energy loss rate. Assuming that the turbulent magnetic field and gas density inside the Cocoon are roughly constant over time, D and b depend only on energy. The computation of the energy loss rate is described below. For selected parameter values of D_0 , Q_0 and α , the gamma ray produced by the electrons are set to explain both the spatial profile and the energy spectrum measured by HAWC.

Following ref. ¹⁰, we consider three radiation fields for γ -ray production: intense stellar light fields surrounding Cyg OB2 and NGC 6910 (a stellar cluster in the vicinity of OB2) and a more diffuse dust radiation field that spans the entire Cocoon. We note that the stellar radiation fields are not important to TeV γ -ray production. The energy of a stellar photon in the rest frame of an electron is $\epsilon'/(m_e c^2) \approx 6 (E_e/1 \text{ TeV}) (T/2 \times 10^4 \text{ K}) \gg 1$, where E_e is the electron energy and T is the temperature of the stars. The inverse-Compton emission at TeV is therefore largely suppressed by the Klein-Nishina effect. By contrast, the dust radiation field peaks at lower frequency and can be upscattered to TeV γ rays. The radiation field is also more extended than the main clusters of Cyg OB2 and NGC 6910. The extended distribution of γ rays alone cannot reject a leptonic scenario in which γ rays are produced by electron-positron pairs.

We compare the synchrotron, Bremsstrahlung and inverse-Compton emission of high-energy electrons with multi-wavelength observations of the Cygnus Cocoon. We find it implausible that a single electron population explains both the GeV to TeV flux and the spatial profile of the γ rays simultaneously, while not violating the X-ray and radio upper limits. Here, we presents a 'minimum leptonic model' (Extended Data Fig. 1) where only γ -ray emission above ~ 1 TeV is explained by electrons. The observed flux between 0.1 GeV and 100 GeV (ref. ¹⁵) is assumed to be produced by hadrons such that they do not contribute to synchrotron radiation at lower energy. Extended Data Fig. 1 shows that even this minimum model can hardly satisfy the constraints posed by multi-wavelength observations.

Deep X-ray observations of the γ -ray Cocoon in the 2–10 keV range¹⁷ and radio flux averaged over the Cocoon from the Canadian Galactic Plane Survey¹⁶ independently constrain the synchrotron emission by relativistic electrons. In addition, relativistic electrons that may explain the HAWC observation between 1 TeV and 100 TeV would unavoidably overproduce a sub-GeV flux of Bremsstrahlung radiation. We therefore conclude that the observed TeV γ rays are more plausibly produced by hadrons. We focus on TeV γ -ray observation in this work, and refer to refs. ^{10,19} for discussion about the origin of the observed GeV γ rays. Future hard X-ray and γ -ray observations resolving subregions of the Cocoon will allow further investigation of the γ -ray production mechanism, which in principle could be a combination of leptonic and hadronic contributions from various stellar activities in the history of the Cocoon.

Summary of systematic uncertainties. The contribution to the systematic uncertainties from the detector effects to the flux normalization of the TeV Cocoon is about $\pm 7\%$ of the nominal value. The index and Gaussian width of the TeV Cocoon change by $<2\%$ because of detector systematics. These uncertainties are determined as described in ref. ²⁹. Further systematic studies were done with a larger ROI without masking 2HWC J2019+367. With a larger ROI, the TeV Cocoon flux normalization and the Gaussian width differ by $<4\%$. The index of the TeV Cocoon differs by $<1\%$. To explore the possible contamination from Galactic diffuse emission and unresolved sources, in addition to the three sources mentioned, a large diffuse emission background is included. It is included in the model either as a Gaussian (spatial morphology) distribution symmetrically distributed about the Galactic latitude of 0° and infinitely extended along Galactic longitude, or as a uniform background with a disk radius of 6° . In both cases, the additional (Galactic diffuse emission and unresolved sources) component is not significantly detected. However, its presence could decrease the Cocoon flux by about 11%. The effects on the index and the Gaussian width are negligible ($<2\%$). In the GeV regime, we studied the Cocoon spectrum published in a 2011 paper¹⁰, the 3FHL catalogue⁵¹ and the 4FGL catalogue¹⁵. The 3FHL and 4FGL catalogues report 10–15% higher flux for the Cocoon compared to the published spectrum in ref. ¹⁰. The results reported in this study are based on the measurements from the 4FGL catalogue¹⁵. Fitting the proton spectrum by using the flux points from ref. ¹⁰ and ref. ⁵¹ and HAWC data results in no significant difference for the total energy of the protons in the Cocoon.

Data availability

The datasets analysed during this study and the scripts used are available at a public data repository (<https://github.com/binitahona/Cocoon-paper>).

Code availability

The study was carried out by using the Analysis and Event Reconstruction Integrated Environment Likelihood Fitting Framework (AERIE-LiFF), the Multi-Mission Maximum Likelihood (3ML) software and the HAWC Accelerated Likelihood (HAL) framework. The code is open-source and publicly available on Github at <https://github.com/rjlauer/aerie-liff>, <https://github.com/threeML/threeML> and https://github.com/threeML/hawc_hal. The software includes instructions on installation and usage.

Received: 16 July 2020; Accepted: 26 January 2021;

Published online: 11 March 2021

References

- Hillas, A. M. in *Composition and Origin of Cosmic Rays* (ed. Shapiro, M. M.) 125 (D. Reidel, 1983).
- Berezinskii, V. S., Bulanov, S. V., Dogiel, V. A. & Ptuskin, V. S. in *Astrophysics of Cosmic Rays* (ed. Ginzburg, V. L.) (North Holland, 1990).
- Baade, W. & Zwicky, F. Cosmic rays from super-novae. *Proc. Natl Acad. Sci. USA* **20**, 259–263 (1934).
- Hörandel, J. R. Models of the knee in the energy spectrum of cosmic rays. *Astropart. Phys.* **21**, 241–265 (2004).
- Bell, A. R., Schure, K. M., Reville, B. & Giacinti, G. Cosmic ray acceleration and escape from supernova remnants. *Mon. Not. R. Astron. Soc.* **431**, 415–429 (2013).
- Aharonian, F. A. Gamma rays from supernova remnants. *Astropart. Phys.* **43**, 71–80 (2013).
- Helder, E. A. et al. Observational signatures of particle acceleration in supernova remnants. *Space Sci. Rev.* **173**, 369–431 (2012).
- Funk, S. in *Handbook of Supernovae* (eds Alsabti, A. W. & Murdin, P.) 1737–1736 (Springer, 2017).
- Abramowski, A. et al. Acceleration of petaelectronvolt protons in the Galactic Centre. *Nature* **531**, 476–479 (2016).
- Ackermann, M. et al. A cocoon of freshly accelerated cosmic rays detected by Fermi in the Cygnus superbubble. *Science* **334**, 1103–1107 (2011).
- Abeysekara, A. U. et al. The 2HWC HAWC observatory gamma-ray catalog. *Astrophys. J.* **843**, 40 (2017).
- Aharonian, F. et al. An unidentified TeV source in the vicinity of Cygnus OB2. *Astron. Astrophys.* **393**, L37–L40 (2002).
- Aharonian, F. et al. The unidentified TeV source (TeV J2032+4130) and surrounding field: final HEGRA IACT-system results. *Astron. Astrophys.* **431**, 197–202 (2005).
- Bartoli, B. et al. Identification of the TeV gamma-ray source ARGO J2031+4157 with the Cygnus Cocoon. *Astrophys. J.* **790**, 152 (2014).
- Abdollahi, S. et al. Fermi Large Area Telescope Fourth Source Catalog. *Astrophys. J. Suppl. Ser.* **247**, 33 (2020).
- Taylor, A. R. et al. The Canadian Galactic Plane Survey. *Astron. J.* **125**, 3145–3164 (2003).
- Mizuno, T. et al. Suzaku observation of the Fermi Cygnus Cocoon: the search for a signature of young cosmic-ray electrons. *Astrophys. J.* **803**, 74 (2015).
- Aguilar, M. et al. Precision measurement of the proton flux in primary cosmic rays from rigidity 1 GV to 1.8 TV with the Alpha Magnetic Spectrometer on the International Space Station. *Phys. Rev. Lett.* **114**, 171103 (2015).
- Aharonian, F., Yang, R. & de Oña Wilhelmi, E. Massive stars as major factories of Galactic cosmic rays. *Nat. Astron.* **3**, 561–567 (2019).
- Aharonian, F. in *Astrophysics at Very High Energies* (eds Walter, R. & Türler, M.) 1–120 (Springer, 2013).
- Wright, N. J., Drew, J. E. & Mohr-Smith, M. The massive star population of Cygnus OB2. *Mon. Not. R. Astron. Soc.* **449**, 741–760 (2015).
- Butt, Y. Beyond the myth of the supernova-remnant origin of cosmic rays. *Nature* **460**, 701–704 (2009).
- Knödlseder, J. Cygnus OB2 – a young globular cluster in the Milky Way. *Astron. Astrophys.* **360**, 539–548 (2000).
- Wright, N. J., Drake, J. J., Drew, J. E. & Vink, J. S. The massive star-forming region Cygnus OB2. II. Integrated stellar properties and the star formation history. *Astrophys. J.* **713**, 871–882 (2010).
- Pinat, E. & Sánchez, J. A. A. Search for extended sources of neutrino emission with 7 years of IceCube data. In *Proc. 35th International Cosmic Ray Conference (ICRC2017)* 963 (PoS, 2017).
- Aartsen, M. G. et al. IceCube-Gen2: The Window to the Extreme Universe. Preprint at <https://arxiv.org/abs/2008.04323> (2020).
- Schoorlemmer, H. A next-generation ground-based wide field-of-view gamma-ray observatory in the southern hemisphere. In *Proc. 36th International Cosmic Ray Conference (ICRC2019)* 785 (PoS, 2019).
- Neronov, A. & Semikoz, D. LHAASO telescope sensitivity to diffuse gamma-ray signals from the Galaxy. *Phys. Rev. D* **102**, 043025 (2020).
- Abeysekara, A. U. et al. Measurement of the Crab Nebula spectrum past 100 TeV with HAWC. *Astrophys. J.* **881**, 134 (2019).
- Abeysekara, A. U. et al. Observation of the Crab Nebula with the HAWC gamma-ray observatory. *Astrophys. J.* **843**, 39 (2017).
- Vianello, G. et al. The Multi-Mission Maximum Likelihood framework (3ML). In *Proc. 7th International Fermi Symposium (IFS2017)* 238 (PoS, 2015).
- Abeysekara, A. U. et al. Multiple galactic sources with emission above 56 TeV detected by HAWC. *Phys. Rev. Lett.* **124**, 021102 (2020).
- Hona, B. Testing the limits of particle acceleration in Cygnus OB2 with HAWC. In *Proc. 36th International Cosmic Ray Conference (ICRC2019)* 699 (PoS, 2019).
- Lang, M. J. et al. Evidence for TeV gamma ray emission from TeV J2032+4130 in Whipple archival data. *Astron. Astrophys.* **423**, 415–419 (2004).
- Albert, J. et al. MAGIC observations of the unidentified γ -ray source TeV J2032+4130. *Astrophys. J. Lett.* **675**, L25 (2008).
- Abdo, A. A. et al. Spectrum and morphology of the two brightest Milagro sources in the Cygnus region: MGRO J2019+37 and MGRO J2031+41. *Astrophys. J.* **753**, 159 (2012).
- Aliu, E. et al. Observations of the unidentified gamma-ray source TeV J2032+4130 by VERITAS. *Astrophys. J.* **783**, 16 (2014).
- Aliu, E. et al. Discovery of TeV gamma-ray emission toward supernova remnant SNR G78.2+2.1. *Astrophys. J.* **770**, 93 (2013).
- Wilks, S. S. The large-sample distribution of the likelihood ratio for testing composite hypotheses. *Ann. Math. Stat.* **9**, 60–62 (1938).
- Fleischhack, H. et al. Modeling the non-thermal emission of the gamma Cygni Supernova Remnant up to the highest energies. In *Proc. 36th International Cosmic Ray Conference (ICRC2019)* 675 (2020).
- Abeysekara, A. U. et al. Extended gamma-ray sources around pulsars constrain the origin of the positron flux at earth. *Science* **358**, 911–914 (2017).
- Knödlseder, J. et al. Gamma-ray line emission from OB associations and young open clusters. II. The Cygnus region. *Astron. Astrophys.* **390**, 945–960 (2002).
- Dermer, C. D. Secondary production of neutral pi-mesons and the diffuse galactic gamma radiation. *Astron. Astrophys.* **157**, 223–229 (1986).
- Kafexhiu, E., Aharonian, F., Taylor, A. M. & Vila, G. S. Parametrization of gamma-ray production cross sections for pp interactions in a broad proton energy range from the kinematic threshold to PeV energies. *Phys. Rev. D* **90**, 123014 (2014).
- Kelner, S. R., Aharonian, F. A. & Bugayov, V. V. Energy spectra of gamma rays, electrons, and neutrinos produced at proton-proton interactions in the very high energy regime. *Phys. Rev. D* **74**, 034018 (2006).
- Syrovatskii, S. I. The distribution of relativistic electrons in the galaxy and the spectrum of synchrotron radio emission. *Sov. Astron.* **3**, 22 (1959).
- Drury, L. O'C. Origin of cosmic rays. *Astropart. Phys.* **39**, 52–60 (2012).
- Me'nik, A. M. & Efremov, Y. N. A new list of OB associations in our Galaxy. *Astron. Lett.* **21**, 10–26 (1995).
- Kharchenko, N. V., Piskunov, A. E., Schilbach, E., Röser, S. & Scholz, R. D. Global survey of star clusters in the Milky Way. II. The catalogue of basic parameters. *Astron. Astrophys.* **558**, A53 (2013).
- Prosekin, A. Y., Kelner, S. R. & Aharonian, F. A. Transition of propagation of relativistic particles from the ballistic to the diffusion regime. *Phys. Rev. D* **92**, 083003 (2015).

51. Ajello, M. et al. 3FHL: the Third Catalog of Hard Fermi-LAT Sources. *Astrophys. J. Suppl. Ser.* **232**, 18 (2017).

Acknowledgements

We acknowledge the support from the United States National Science Foundation; the United States Department of Energy Office of High-Energy Physics; the Laboratory Directed Research and Development program of Los Alamos National Laboratory; Consejo Nacional de Ciencia y Tecnología in Mexico, grant nos. 271051, 232656, 260378, 179588, 254964, 258865, 243290, 132197, A1-S-46288 and A1-S-22784, cátedras 873, 1563, 341 and 323, Red HAWC, Mexico; Dirección General Asuntos del Personal Académico, Universidad Nacional Autónoma de México, grant nos. IG101320, IN111315, IN111716-3, IN111419, IA102019 and IN112218; Vicerrectoría de Investigación y Estudios de Posgrado de la Benemérita Universidad Autónoma de Puebla; Programa Integral de Fortalecimiento Institucional (PIFI) 2012–2013 and Programa de Fortalecimiento de la Calidad Educativa (PROFOCIE) 2014–2015; the University of Wisconsin Alumni Research Foundation; the Institute of Geophysics, Planetary Physics, and Signatures at Los Alamos National Laboratory; the Polish Science Centre, grant no. DEC-2017/27/B/ST9/02272; Coordinación de la Investigación Científica de la Universidad Michoacana; Coordinación General Académica y de Innovación (CGAI-UDG; SEP-PRODEP-UDG-CA-499); the Royal Society, Newton Advanced Fellowship 180385; and Generalitat Valenciana, grant no. CIDEGENT/2018/034. We thank S. Delay, L. Díaz and E. Murrieta for technical support, and thank S. Digel for helpful discussion regarding the source modelling of the Cygnus Cocoon region in the Fermi 4FGL catalogue.

Author contributions

B.H. analysed the HAWC data and performed the maximum-likelihood fit of the multi-source model, the hadronic model fit and the cosmic ray density study. H.F. and P.H. helped in the development of the multi-source model and in the scientific interpretations

of the fit results. K.F. and R.B. helped develop the hadronic emission models and helped in the interpretations of the model fit results. K.F. also developed the leptonic emission model and provided its interpretations. S.C. motivated the Cocoon analysis, helped with the interpretations of the leptonic model and performed the diffusion coefficient suppression study at the Cocoon region. B.H., K.F. and S.C. prepared the manuscript. The full HAWC Collaboration group contributed through the construction, calibration and operation of the detector, the development and maintenance of reconstruction and analysis software, and the vetting of the analysis presented in this manuscript. All authors reviewed, discussed and commented on the results and the manuscript.

Competing interests

The authors declare no competing interests.

Additional information

Extended data is available for this paper at <https://doi.org/10.1038/s41550-021-01318-y>.

Supplementary information The online version contains supplementary material available at <https://doi.org/10.1038/s41550-021-01318-y>.

Correspondence and requests for materials should be addressed to R.B., S.C., K.F., H.F., B.H. and P.H.

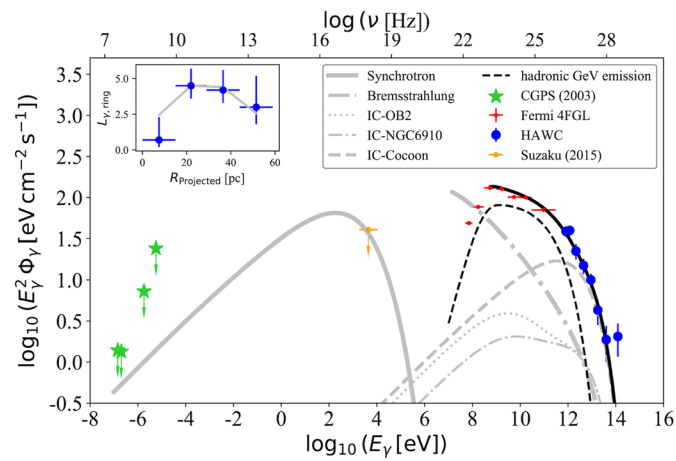
Peer review information *Nature Astronomy* thanks Songzhan Chen, Emma de Oña Wilhelmi and the other, anonymous, reviewer(s) for their contribution to the peer review of this work.

Reprints and permissions information is available at www.nature.com/reprints.

Publisher's note Springer Nature remains neutral with regard to jurisdictional claims in published maps and institutional affiliations.

© The Author(s), under exclusive licence to Springer Nature Limited 2021, corrected publication 2021

¹Department of Physics and Astronomy, University of Utah, Salt Lake City, UT, USA. ²Physics Division, Los Alamos National Laboratory, Los Alamos, NM, USA. ³Instituto de Física, Universidad Nacional Autónoma de México, Mexico City, Mexico. ⁴Universidad Autónoma de Chiapas, Tuxtla Gutiérrez, Mexico. ⁵Universidad Michoacana de San Nicolás de Hidalgo, Morelia, Mexico. ⁶Instituto de Geofísica, Universidad Nacional Autónoma de México, Mexico City, Mexico. ⁷Department of Physics, Pennsylvania State University, University Park, PA, USA. ⁸Institute of Nuclear Physics Polish Academy of Sciences, Krakow, Poland. ⁹Department of Physics and Astronomy, University of Rochester, Rochester, NY, USA. ¹⁰Department of Physics, Stanford University, Stanford, CA, USA. ¹¹Department of Physics, University of Maryland, College Park, MD, USA. ¹²Instituto Nacional de Astrofísica, Óptica y Electrónica, Puebla, Mexico. ¹³Instituto de Astronomía, Universidad Nacional Autónoma de México, Mexico City, Mexico. ¹⁴Departamento de Física, Centro Universitario de Ciencias Exactas e Ingenierías, Universidad de Guadalajara, Guadalajara, Mexico. ¹⁵Institute for Cosmic Ray Research, University of Tokyo, Kashiwa, Kashiwanoha, Japan. ¹⁶Department of Physics, University of Wisconsin–Madison, Madison, WI, USA. ¹⁷Department of Physics, Michigan Technological University, Houghton, MI, USA. ¹⁸Max Planck Institute for Nuclear Physics, Heidelberg, Germany. ¹⁹Department of Physics, Faculty of Science, Chulalongkorn University, Bangkok, Thailand. ²⁰National Astronomical Research Institute of Thailand, Chiang Mai, Thailand. ²¹Erlangen Centre for Astroparticle Physics, Friedrich-Alexander-Universität Erlangen-Nürnberg, Erlangen, Germany. ²²Department of Physics and Astronomy, Michigan State University, East Lansing, MI, USA. ²³Universidad Politécnica de Pachuca, Pachuca, Mexico. ²⁴Facultad de Ciencias Físico Matemáticas, Benemérita Universidad Autónoma de Puebla, Puebla, Mexico. ²⁵Centro de Investigación en Computación, Instituto Politécnico Nacional, Mexico City, Mexico. ²⁶Department of Physics and Astronomy, University of New Mexico, Albuquerque, NM, USA. ²⁷Universidad Autónoma del Estado de Hidalgo, Pachuca, Mexico. ²⁸Instituto de Ciencias Nucleares, Universidad Nacional Autónoma de México, Mexico City, Mexico. ²⁹Natural Science Research Institute, University of Seoul, Seoul, Republic of Korea. ³⁰Instituto de Física Corpuscular, CSIC, Universitat de València, Valencia, Spain. ³¹Department of Chemistry and Physics, California University of Pennsylvania, California, PA, USA. ³²Departamento de Física, Centro de Investigación y de Estudios Avanzados del IPN, Mexico City, Mexico. ³³Tsung-Dao Lee Institute and School of Physics and Astronomy, Shanghai Jiao Tong University, Shanghai, China. ✉e-mail: rdb3@stanford.edu; sabrina.casanova@ifj.edu.pl; kefang@physics.wisc.edu; hfleisch@mtu.edu; bhona@mtu.edu; petra@mtu.edu



Extended Data Fig. 1 | Leptonic modelling at the Cocoon region. Multi-wavelength observations of the Cygnus Cocoon (15; 17; 19) constrain the Synchrotron and Bremsstrahlung radiation of relativistic electrons. The light grey curves correspond to a ‘minimum leptonic model’, where only γ -rays above 1 TeV are explained by electron emission. The electron population is assumed to follow a power-law energy spectrum $dN/dE \propto E^{-2}$ in a region with magnetic field $B = 20 \mu\text{G}$ and gas density $n = 30 \text{ cm}^{-3}$ as in the Cocoon (10). The leptonic emission consists of the Synchrotron radiation (solid, from radio to hard X-ray), Bremsstrahlung emission (thick dash-dotted), and inverse-Compton scattering of the dust emission in the Cocoon (dashed) and the radiation fields of the two stellar clusters, NGC 6910 (thin dash-dotted) and OB2 (dotted). Observations between 0.1–100 GeV are explained by hadronic interaction (black dashed curve). The red points are the GeV flux points by Fermi-LAT and the blue circles are the HAWC flux points with 1σ statistical errors. The sum of the emission above ~ 0.3 GeV is indicated by the black solid curve. In the inner plot, the blue circles indicate the γ -ray luminosity for the four rings at the Cocoon region and the light grey solid curve is the TeV γ -ray luminosity from the model.